

Grover's search meets Ising models: a quantum algorithm for finding low-energy states

A. A. Zhukov¹, A. V. Lebedev^{1,2}, W. V. Pogosov^{1,2,3}

¹*Dukhov Research Institute of Automatics (VNIIA), Moscow, 127030, Russia*

²*Advanced Mesoscience and Nanotechnology Centre,
Moscow Institute of Physics and Technology (MIPT), Dolgoprudny, 141700, Russia and*

³*Institute for Theoretical and Applied Electrodynamics,
Russian Academy of Sciences, Moscow, 125412, Russia*

We propose a methodology for implementing Grover's algorithm in the digital quantum simulation of disordered Ising models. The core concept revolves around using the evolution operator for the Ising model as the quantum oracle within Grover's search. This operator induces phase shifts for the eigenstates of the Ising Hamiltonian, with the most pronounced shifts occurring for the lowest and highest energy states. Determining these states for a disordered Ising Hamiltonian using classical methods presents an exponentially complex challenge with respect to the number of spins (or qubits) involved. Within our proposed approach, we determine the optimal evolution time by ensuring a phase flip for the target states. This method yields a quadratic speedup compared to classical computation methods and enables the identification of the lowest and highest energy states (or neighboring states) with a high probability $\lesssim 1$.

PACS numbers:

I. INTRODUCTION

In recent years, significant advancements have been made in the development of real quantum computers using various physical platforms [1–4]. Among the promising applications of quantum computing, quantum simulation stands out [5, 6]. Quantum computing offers advantages such as an exponentially larger Hilbert space compared to classical systems and the ability to utilize quantum phenomena like quantum interference and parallelism [7]. These features are also instrumental in achieving exponential or polynomial speedups in quantum algorithms like Shor's and Grover's algorithms [8, 9]. For recent advancements in Grover's algorithm, see, e.g., Refs. [10–14].

This paper aims to integrate Grover's search with quantum simulation of classical spin models such as the Ising model. It is well-established that many NP-complete and NP-hard problems can be framed in terms of Ising models [15, 16]. A crucial element of Grover's algorithm is the quantum oracle, which alters the phase of the target state. We propose an analogy between this oracle and the evolution operator of the Ising Hamiltonian, which similarly modifies the phases of eigenstates in the uniform superposition depending on their energies and time. By identifying the optimal evolution time that flips the phases of the lowest or highest energy states, we can enhance the probability of finding these states in the superposition, akin to Grover's search. Additionally, we can use another evolution time to amplify probability amplitudes around arbitrary energies to target corresponding quantum states.

As a case study, we examine a disordered classical Ising model with all-to-all interactions and random energy constants. Our algorithm effectively operates as Grover's search, enabling the identification of target eigenstates or those closely related to them in energy with high probability ($\lesssim 1$). Consequently, our approach offers a quadratic speedup compared to classical brute-force search and may present a viable alternative to other quantum simulation methods for Ising model, such as quantum annealing [17–19] or variational quantum algorithms [20, 21]. Note that our method is particularly relevant for the era of fault-tolerant quantum computing, as Grover's algorithm is known to be sensitive to gate errors [22].

The paper is structured as follows. In Section II, we formulate our method. Section III presents our main results. We conclude in Section IV.

II. METHOD

A. Hamiltonian

In our scenario, spins can be naturally represented by qubits. The Hamiltonian of the classical Ising model is expressed as follows:

$$H_{\text{Ising}} = \sum_{j=1}^{N_q} \varepsilon_j \sigma_j^z + \sum_{i \neq j}^{N_q} J_{ij} \sigma_i^z \sigma_j^z, \quad (1)$$

where σ_j^z denotes the Z -Pauli operator acting on the j -th spin (qubit), and N_q represents the number of qubits. The total number of eigenstates of the Ising Hamiltonian is given by $N_s = 2^{N_q}$. The energy constants follow a random distribution, typically a Gaussian distribution. Here, we assume $\bar{\varepsilon} = \bar{J} = 0$, where the averaging is carried out over the qubits, and the standard deviations for J_{ij} and ε_j are denoted by $\sigma_J = \sigma_\varepsilon = 2$.

It is worth noting that our methodology extends naturally to more complex Ising model variants [23], which incorporate higher-order terms such as $\sim \sigma_i^z \sigma_j^z \sigma_k^z$, and so forth.

B. Algorithm

The algorithm comprises the following steps:

Firstly, we initialize the qubits in the register by applying Hadamard gates to each qubit, resulting in the uniform superposition of all eigenstates of the Ising Hamiltonian:

$$|s\rangle = \frac{1}{\sqrt{N_s}} \sum_{j=1}^{N_s} |j\rangle. \quad (2)$$

Subsequently, we perform Grover's iteration n times, with each iteration consisting of two sub-steps:

(i) Application of the quantum oracle. This oracle is represented by the evolution operator for the Ising Hamiltonian corresponding to a fixed time T , given by:

$$U_{\text{Ising}} = \exp(-iH_{\text{Ising}}T). \quad (3)$$

The operator U_{Ising} can be trivially represented using R_z and R_{zz} rotation gates, and there is no need for Trotterization, as all contributions to the Hamiltonian in Eq. (1) commute with each other.

Specifically, after the first application of the oracle, the state becomes:

$$\frac{1}{\sqrt{N_s}} \sum_{j=1}^{N_s} \exp(-iE_j T) |j\rangle, \quad (4)$$

where E_j represents the eigenenergy corresponding to the eigenstate $|j\rangle$. Consequently, the oracle induces phase shifts that are most pronounced for the lowest energy and highest energy eigenstates.

(ii) Application of Grover's diffusion operator, defined conventionally as:

$$U_{\text{Grover}} = 2|s\rangle\langle s| - I. \quad (5)$$

The role of this operator is to enhance the probability amplitudes for the lowest energy and highest energy states,

where the phase shift is optimal, nearly corresponding to a phase flip akin to the usual Grover's search.

Our algorithm introduces two independent controlling parameters: T and n , unlike the traditional Grover's algorithm characterized by a single parameter n . The selection of these two parameters is discussed in the subsequent subsections.

C. Optimal mean evolution time T

Let us estimate a ground state energy, which allows to evaluate the optimal evolution time.

For large values of N_s , the eigenenergies can be described by a probability density function given a specific set of ε_j and J_{ij} , corresponding to a particular disorder realization. In our case, the eigenenergies follow a Gaussian distribution with a mean value of zero. The probability density function is represented as:

$$f(E) = \frac{1}{\sigma\sqrt{2\pi}} \exp\left(-\frac{E^2}{2\sigma^2}\right), \quad (6)$$

where σ denotes the standard deviation, which can be determined classically by evaluating a number of eigenstates E_j using the Monte Carlo method.

To estimate the lowest energy E_{\min}^* and highest energy E_{\max}^* based on the probability density function in Eq. (6), we solve the following equations:

$$N_s \int_{-\infty}^{E_{\min}^*} f(x) dx = 1, \quad (7)$$

and

$$N_s \int_{E_{\max}^*}^{\infty} f(x) dx = 1. \quad (8)$$

Introducing dimensionless quantities $e_{\min}^* = E_{\min}^*/\sigma$ and $e_{\max}^* = E_{\max}^*/\sigma$, we readily find that $e_{\max}^* = -e_{\min}^*$. Solving for e_{\min}^* , we obtain:

$$\frac{1}{2} \operatorname{erfc} \frac{|e_{\min}^*|}{\sqrt{2}} = 2^{-N_q}, \quad (9)$$

where erfc represents the complementary error function.

The estimate of the optimal evolution time T^* is derived from the condition of the phase flip for the lowest and highest energy states:

$$|E_{\min}^*| T^* = \pi, \quad (10)$$

resulting in:

$$T^* = \frac{\pi}{\sigma} \frac{1}{|e_{\min}^*|}. \quad (11)$$

For large N_q , an asymptotic expansion for the complementary error function in Eq. (9) yields the approximate expression for T^* :

$$T^* \simeq \frac{1}{\sigma} \frac{\pi}{\sqrt{2 \ln 2}} \frac{1}{\sqrt{N_q}} \left(1 + \frac{1}{4 \ln 2} \frac{\ln N_q}{N_q} \right). \quad (12)$$

Utilizing T^* from Eqs. (11) and (9) allows us to enhance probability amplitudes for eigenstates E_j located at the tails of the distribution, where only a countable number of eigenenergies typically reside. However, it is essential to note that T^* represents the mean optimal time averaged over realizations of disorder, rather than the true optimal evolution time T_{opt} , which fluctuates depending on the precise values of E_{min} and E_{max} . In this sense, T^* reflects the mean optimal time T_{opt} averaged over the realizations of disorder. The latter is demonstrated numerically in the subsequent section, showcasing excellent agreement between the results of numerical computation and theory. To fine-tune the optimal time and target the true lowest energy or highest energy states, methods such as Monte Carlo simulations can be employed to sample values of time in the vicinity of T^* given by Eqs. (11) and (9).

It is worth noting that our approach can be extended to target states with energies E_{tar} different from E_{max} and E_{min} . This can be achieved by adopting the evolution time $\pi/|E_{\text{tar}}|$, amplifying probability amplitudes for states with energies in the vicinity of E_{tar} . Generally, probabilities for all states with energies $E_{\text{tar}}(2l+1)$ will be amplified, where l is an integer number.

D. Optimal mean iteration number n

In the conventional Grover's search, the optimal number n^* of iterations is determined by [9]

$$\sin^2(2n^* + 1)a \simeq 1, \quad (13)$$

where $a = \arcsin(1/\sqrt{N_s})$. For large N_s , this leads to $n^* \simeq \frac{\pi}{4}\sqrt{N_s}$, showcasing a quadratic speedup compared to classical search algorithms.

Numerical investigations (as detailed in the subsequent section) reveal that our proposed approach yields results consistent with Eq. (13). Specifically, the optimal n_{opt} averaged over different realizations of disorder agree well with the predictions of Eq. (13).

III. MAIN RESULTS

A. Probability amplitudes

Consider the state after the first Grover's iteration, employing the quantum oracle provided by the evolution operator of the Ising model. It can be expressed as

$$|\psi^{(1)}\rangle = \sum_{j=1}^{N_s} g_j^{(1)} |j\rangle, \quad (14)$$

where

$$g_j^{(1)} = \frac{2}{N_s \sqrt{N_s}} \sum_{k=1}^{N_s} e^{-iE_k T} - \frac{1}{\sqrt{N_s}} e^{-iE_j T}. \quad (15)$$

For the disordered Ising model under consideration, in the leading order of N_s , the sum in the right-hand side of this equation can be replaced by an integral, yielding

$$\sum_{k=1}^{N_s} e^{-iE_k T} \simeq N_s \int_{-\infty}^{+\infty} f(E) e^{-iET} dE = N_s e^{-\sigma^2 T^2 / 2}. \quad (16)$$

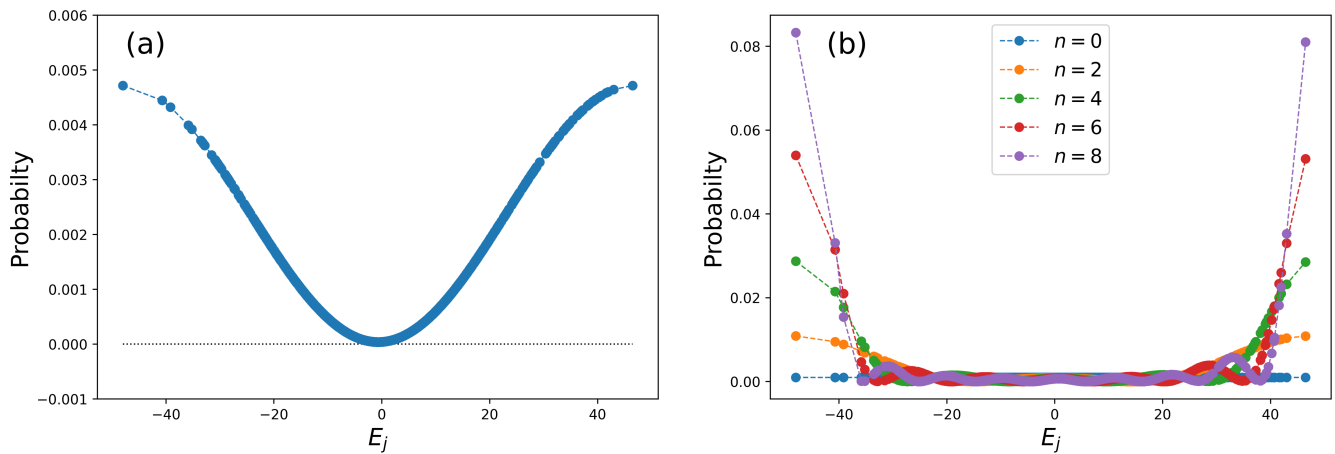


Fig. 1: Probability of finding the state with energy E_j after the first Grover's iteration at $N_q = 10$ (a); the same quantity, but after the n -th Grover's iteration (b). Dotted lines are guides for the eyes connecting points, which correspond to discrete eigenenergies.

Thus, we have

$$g_j^{(1)} \simeq \frac{1}{\sqrt{N_s}} (2e^{-\sigma^2 T^2/2} - e^{-iE_j T}). \quad (17)$$

The first term in the right-hand side of this equation is real, while the second term, in general, is complex. However, the second term also becomes nearly real and approaches -1 for E_j in the vicinity of E_{max} and E_{min} . This interplay amplifies the overall probability for the eigenenergies residing at the tails of the original distribution. In contrast, $\exp(-iE_j T)$ is nearly equal to 1 for $E_j \simeq 0$, leading to the suppression of the corresponding probability. Thus, the underlying mechanism of the algorithm can be understood in terms of positive and negative quantum interference. This scenario is valid for any distribution of eigenenergies which is symmetric relative to the vertical axis.

By induction, it can be shown that the state after the n -th Grover's iteration can be represented as

$$|\psi^{(n)}\rangle = \sum_{j=1}^{N_s} g_j^{(n)} |j\rangle, \quad (18)$$

where $g_j^{(n)}$ satisfies a recurrent relation

$$g_j^{(n)} = \frac{2}{N_s} \sum_{k=1}^{N_s} e^{-iE_k T} g_k^{(n-1)} - e^{-iE_j T} g_j^{(n-1)}, \quad (19)$$

with $g_j^{(0)} = 1/\sqrt{N_s}$. Since at any iteration $g_j^{(n)}$ is symmetric relative to the vertical axis, the condition of probability amplification is the same as the one at $n = 1$.

Figure 1 (a) illustrates the dependence of $|g_j^{(1)}|^2$, representing the probability of measuring the state $|j\rangle$ after the first iteration, on E_j for $N_q = 10$, $T = T^*$, and a specific disorder realization. To conduct these computations, the set of E_j was initially computed for a given set of ε_j, J_{ij} . As observed from this figure, the probability of measuring eigenstates at the tails of the distribution is amplified, while the same probability for "inner" states is suppressed. Subsequent Grover's iterations further concentrate this distribution towards the tails of the original Gaussian distribution of eigenenergies, as depicted in Figure 1 (b) for $|g_j^{(n)}|^2$ and various values of n . These calculations were performed numerically using Eq. (19) for the same disorder realization. Dotted lines are included as guides for

the eyes connecting points corresponding to discrete eigenenergies.

Let us now adopt a slightly different perspective on the problem. At k -th step of the Grover's procedure the quantum state of the system can be presented as

$$|\psi^{(n)}\rangle = a_{\pm}^{(n)}|\pm\rangle + \sum_{k=0}^n b_k^{(n)}|k\rangle, \quad (20)$$

where $|\pm\rangle$ is a superposition of two extreme energy states $|\pm\rangle = [| + E_{\min}\rangle + | - E_{\min}\rangle]/\sqrt{2}$, $|k\rangle = \hat{U}_{\text{Ising}}^k|0\rangle$ where

$$|0\rangle = \frac{1}{\sqrt{N_s - 2}} \sum_{j \neq \pm} |E_j\rangle, \quad (21)$$

is an equal weights superposition of all non extreme states of the system.

After the Grover iteration at the optimal time duration $T = T^*$ the state $|\psi^{(n)}\rangle$ experiences a sequence of transformations:

$$\hat{U}_{\text{Ising}}|\psi^{(n)}\rangle = -a_{\pm}^{(n)}|\pm\rangle + \sum_{k=0}^n b_k^{(n)}|k+1\rangle, \quad (22)$$

$$\begin{aligned} \hat{U}_{\text{Grover}}\hat{U}_{\text{Ising}}|\psi^{(n)}\rangle &= a_{\pm}^{(n)}|\pm\rangle \left[(1 - 2a_0^2)|\pm\rangle + \sum_{k=0}^n b_k^{(n)} 2a_0b_0\langle 0|k+1\rangle \right] \\ &+ |0\rangle \left[-2a_0b_0a_{\pm}^{(n)} + \sum_{k=0}^n b_k^{(n)} 2b_0^2\langle 0|k+1\rangle \right] - \sum_{k=0}^n b_k^{(n)}|k+1\rangle, \end{aligned} \quad (23)$$

where $a_0 = \sqrt{2/N_s}$, $b_0 = \sqrt{1 - a_0^2}$. One can see, that during the Grover's iteration the vector $\vec{a}^{(n)} \equiv (a_{\pm}^{(n)}, b_0^{(n)}, b_1^{(n)}, \dots)$ composed of the state $|\psi^{(n)}\rangle$ amplitudes, see Eq. (20), experiences the linear transformation: $\vec{a}^{(n)} \rightarrow \vec{a}^{(n+1)} = \hat{G} \cdot \vec{a}^{(n)}$, described by the matrix

$$\hat{G} = \begin{bmatrix} 1 - 2a_0^2 & 2a_0b_0\langle 0|1\rangle & 2a_0b_0\langle 0|2\rangle & \dots & \dots \\ -2a_0b_0 & 2b_0^2\langle 0|1\rangle & 2b_0^2\langle 0|2\rangle & \dots & \dots \\ 0 & -1 & 0 & \dots & \dots \\ 0 & 0 & -1 & 0 & \dots \\ \dots & \dots & \dots & \dots & \dots \end{bmatrix}. \quad (24)$$

Therefore, after n Grover's iterations the quantum state of the system is described by the amplitude vector $\vec{a}^{(n)} = \hat{G}^n \cdot \vec{a}^{(0)}$ of the length $n+2$ with the initial condition $\vec{a}^{(0)} = (a_0, b_0, 0, \dots)$. For the disordered Ising model all statistics of the energy levels is hidden into the overlap amplitudes $\langle 0|k\rangle$,

$$\langle 0|k\rangle = \frac{1}{N_s - 2} \sum_{j \neq \pm} e^{-ikE_j T}, \quad (25)$$

which at large N_s can be considered as an average over the energy levels statistical distribution $f(E)$,

$$\langle 0|k\rangle \approx \int dE f(E) e^{-ikET}. \quad (26)$$

Assuming the Gaussian distribution $f(E)$, see Eq.(6), one gets the overlaps $\langle 0|k\rangle$ exponentially vanish with k ,

$$\langle 0|k\rangle = \exp\left(-\frac{1}{2}k^2T^2\sigma^2\right) = \exp\left(-\frac{\pi^2k^2}{2}\frac{\sigma^2}{E_{\min}^2}\right). \quad (27)$$

The computational scheme employing the \hat{G}^n linear transformation of the initial amplitude vector \vec{a}_0 allows us calculate the dynamics of the success probability $P_{\pm}^{(n)} = |a_{\pm}^{(n)}|^2$ to find correct extreme energy state $\pm E_{\min}$ during the Grover's procedure for any statistical distribution $f(E)$ of the energy spectrum. This scheme turns out to be more efficient than a direct step by step update of the state amplitudes according to Eq.(19), as it requires to keep only $\mathcal{O}(\sqrt{N_s})$ vector $\vec{a}^{(n)}$ and sparse square matrix \hat{G} of the same size.

To demonstrate the performance of the Grover's procedure, we plot the dynamics of the probability $P_{\pm}^{(n)}$ at different steps n of the Grover's procedure and at different levels of disorder σ of the Gaussian distribution $f(E)$ of the energy levels, as shown in Fig. 2. It can be observed that the Grover's procedure indeed leads to an enhancement in the success probability after $n^* = \frac{\pi}{4}\sqrt{N_s/2}$ iterations, where the factor 2 in the square root accounts for the phase degeneracy of two extreme states after Ising evolution: $\hat{U}_{\text{Ising}}|\pm E_{\min}\rangle = -|\pm E_{\min}\rangle$.

The maximal success probability decreases both with the increase in disorder and the number of qubits. As the disorder increases, the probability of obtaining an energy state close to the extreme states also increases, and the Grover's procedure enhances the amplitude of this state, thereby reducing the amplitudes of the extreme states. Similarly, the same effect occurs with the increase in system size.

In running Grover's search, we must preselect the number of Grover iterations n^* under the assumption of the absence of energy states proximal to the extreme states. However, this assumption may not hold true due to our lack of knowledge regarding the actual energy state distribution. Consequently, one or more states may appear nearby. To assess the impact of closely lying states on the success probability, we sample the energy state distribution with one state positioned at an energy distance $\Delta > 0$ above the minimal energy state $-|E_{\min}|$. It is observed that the success probability $P_{\pm}^{(n^*)}$ at the optimal Grover iteration number n^* as a function of Δ saturates at $\Delta T^* n^* > 2\pi$, as illustrated in Fig. 3. Notably, in the dimensionless rescaled gap variable $\delta \equiv \Delta T^* n^* / \pi$, the dependence $P_{\pm}^{(n^*)}(\delta)$ aligns with a universal curve across all system sizes. Consequently, one may argue that the critical value of the energy gap Δ^* , where the success probability becomes nonsensitive to the presence of closely lying levels, diminishes with the system size as,

$$\Delta^* \sim \frac{2\pi}{T^* n^*} \propto \frac{1}{\sqrt{N_s}}. \quad (28)$$

B. Fixed evolution time and iteration number

Now, we present our results obtained using a quantum computer simulator. We utilized qiskit to simulate the quantum circuits, representing the evolution operator in the standard form using R_z and R_{zz} rotation gates.

In this subsection, we consider a fixed evolution time T^* given by Eqs. (11) and (9), and a fixed number of Grover's iterations n^* given by Eq. (13). Thus, we assume a given set of parameters ε_j and J_{ij} , which lead to a certain σ . The latter is supposed to be known. Under these assumptions, we ran the search algorithm for fixed $T = T^*$ and $n = n^*$.

Firstly, we examine the probability P_j of obtaining the eigenstate of H corresponding to the eigenenergy E_j . The values of P_j versus E_j are depicted in Fig. 4 (a) for 400 different realizations of disorder at $N_q = 13$. Two peaks corresponding to the tails of the initial Gaussian distribution are observed. However, the maximum energy and minimum energy states vary for different realizations of disorder, which somewhat obscures the effect of probability amplification in Fig. 4 (a). For this reason, in Fig. 4 (b), we plot the same quantity as a function of ξ_j , where

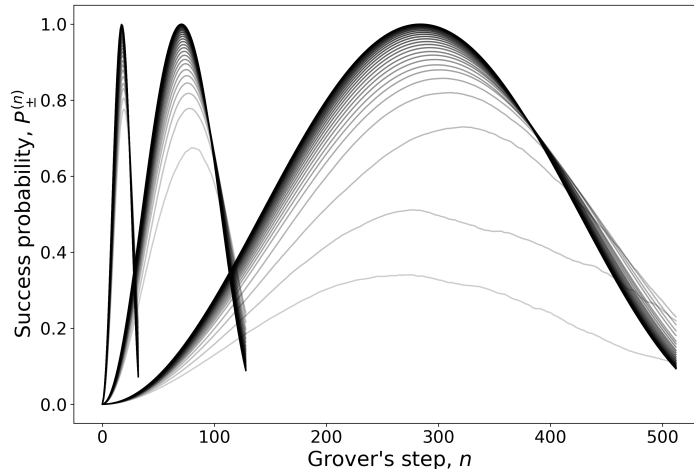


Fig. 2: Evolution of the success probability P_n for $N_q = 10, 14$ and 18 at different levels of the disorder σ ranging from $\sigma T^* = 0.01\pi$ to $\sigma T^* = 0.25\pi$. The disorder level is marked by the contrast with higher contrast corresponding to a lower disorder level. Each curve was built by averaging over 400 realizations of the energy spectrum each sampled from the normal distribution $\mathcal{N}(0, \sigma)$.

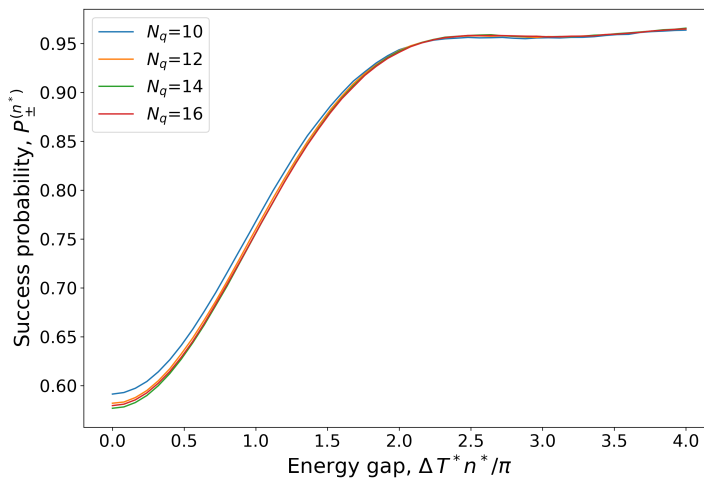


Fig. 3: The success probability at the optimal Grover iteration number n^* as a function of the dimensionless energy gap $\delta = \Delta T^* n^* / \pi$ between the lowest and the next energy state at different system size.

ξ_j is a realization-dependent quantity given by $\xi_j = (E_j - E_{min}) / (E_{max} - E_{min})$. This quantity is exactly 0 for $E_j = E_{min}$ and exactly 1 for $E_j = E_{max}$. We observe that two peaks at 0 and 1 emerge in this plot, demonstrating the amplification of probabilities at the tails of the distribution.

It is also of interest to explore the same probability P_j but multiplied by the density of states. This quantity, denoted as $P'(E)$, gives the probability density function of obtaining the state with energy E at the end of the algorithm. This characteristic for $N_q = 13$ is shown in Fig. 5 (a) in a histogram form by the blue color for 400 realizations of disorder. The initial distribution is also displayed by the dashed black line. Figure 5 (b) presents the same quantity but as a function of ξ , where the peak structure is more pronounced.

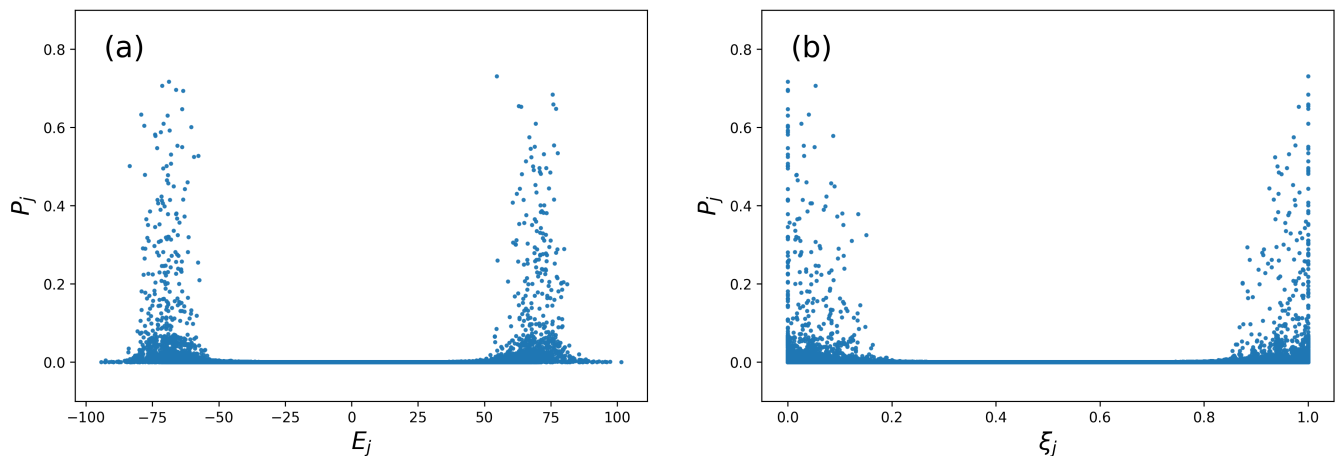


Fig. 4: (a) Probability P_j versus E_j at $N_q = 13$ for 400 realizations of disorder. (b) Probability P_j versus ξ_j for the same set of parameters. Both T and n are fixed and equal to T^* and n^* , respectively.

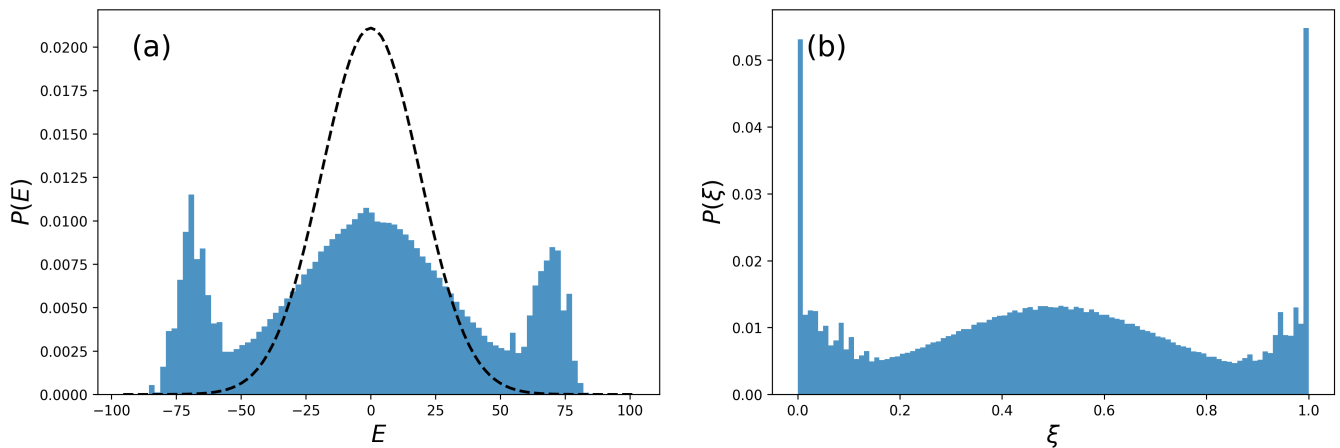


Fig. 5: (a) Histogram showing the probability $P'(E)$ (blue color) at $N_q = 13$, averaged over 400 realizations of disorder. For comparison, also shown is the initial distribution (dashed black line). (b) Histogram showing the probability $P'(\xi)$ (blue color) for the same set of parameters. Both T and n are fixed and equal to T^* and n^* , respectively.

C. Fine tuning of controlling parameters

In this subsection, we explore the tuning of the main controlling parameters T and n depending on the realization of disorder, i.e., for different sets of ε_j and J_{ij} with the same normal distribution. Initially, we present our results corresponding to the tuned evolution time, while n is assumed to be fixed at $n = n^*$. The optimal time T_{opt} can be found by adjusting T in the vicinity of T^* and measuring the probabilities of obtaining different states at the end of the algorithm. The value of T that maximizes the probability of measuring the state with the maximum $|E_j|$ corresponds to T_{opt} . Figure 6 (a) displays P_j versus E_j at $T = T_{opt}$ and $N_q = 13$ for 400 realizations of disorder, while Fig. 6(b) illustrates P_j versus ξ_j . The peaks in these figures are more pronounced compared to similar peaks in Fig. 4. The same is true for P'_j , as shown in Fig. 7 for $N_q = 13$.

We also compare the true optimal evolution time \bar{T}_{opt} averaged over realizations of disorder with T^* evaluated numerically from Eqs. (9) and (12). The results are presented in Fig. 8 for different qubit numbers N_q . Lines serve as guides for the eyes, connecting discrete points corresponding to different qubit numbers. We observe an excellent

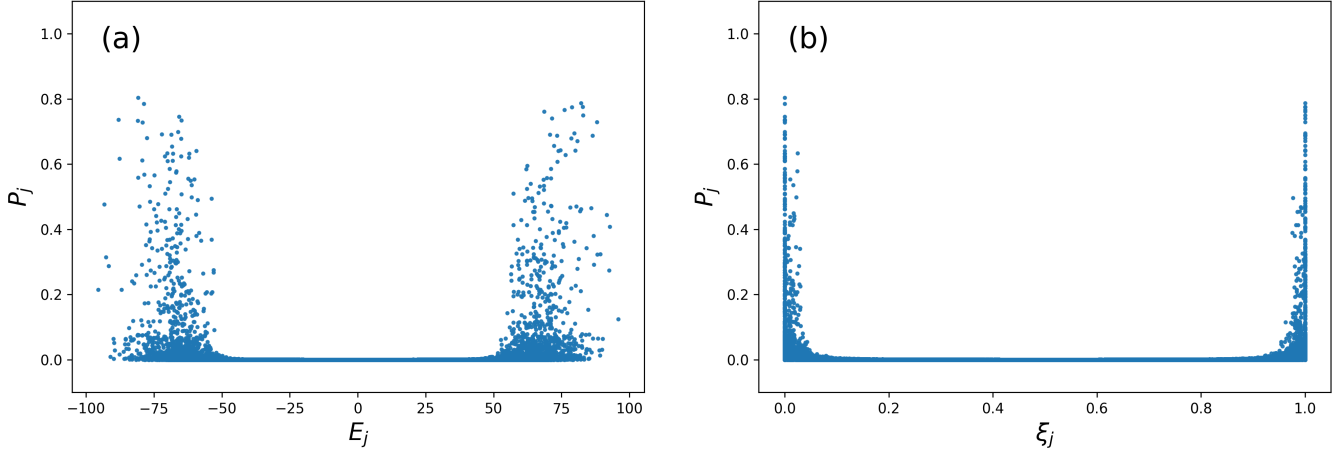


Fig. 6: (a) Probability P_j versus E_j at $N_q = 13$ for 400 realizations of disorder. (b) Probability P_j versus ξ_j for the same set of parameters. Fine tuning of T is adopted.

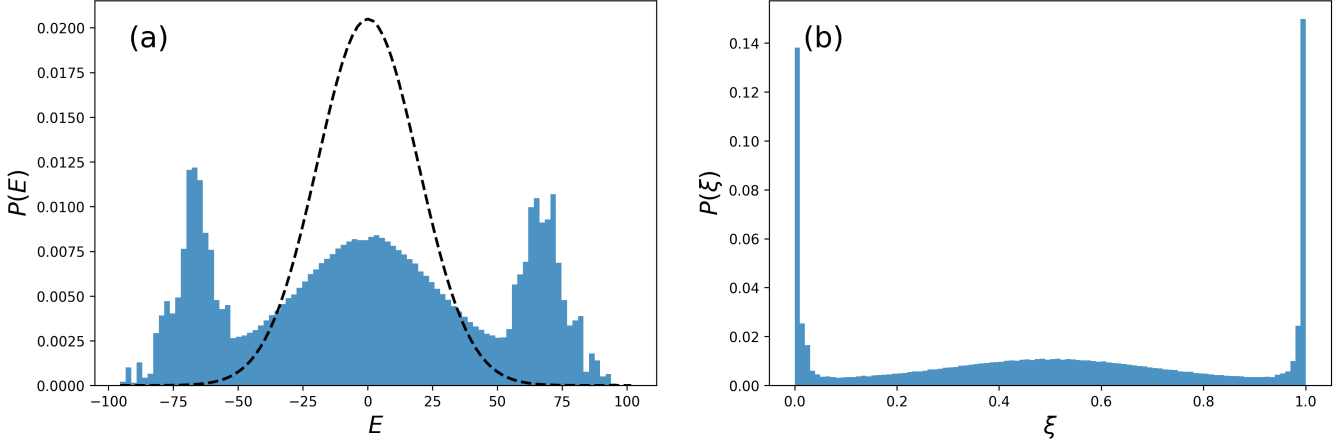


Fig. 7: (a) Histogram showing the probability $P'(E)$ (blue color) at $N_q = 13$, averaged over 400 realizations of disorder. For comparison, the initial distribution is also shown (dashed black line). (b) Histogram showing the probability $P'(\xi)$ (blue color) for the same set of parameters. Evolution time T is tuned for each realization of disorder, while $n = n^*$.

agreement between the theory and the results of the numerical experiments.

Figure 9 illustrates the dependence of the probability of obtaining the state with the maximum $|E_j|$ as a function of time T for $N_q = 6$ and 100 realizations of disorder. Dots indicate the maxima of these dependencies, which correspond to the true optimal evolution time T_{opt} . Furthermore, Fig. 10 presents the probability of obtaining the state with the maximum $|E_j|$ measured at the optimal time $T = T_{opt}$ for different Grover's iteration numbers n , $N_q = 7$, and 100 realizations of disorder. Blue dots represent data averaged over the realizations of disorder, with the blue dashed line serving as a guide for the eyes connecting discrete points. The first peak on this dependence corresponds to 10 Grover's iterations, while, according to Eq. (13), $n^* = 9$ Grover's iterations are optimal. The difference between these numbers is small which demonstrates that our method operates similarly to Grover's search.

Lastly, we consider tuning not only the evolution time around T^* , but also tuning the Grover's iteration number around n^* for each realization of disorder. This allows us to achieve realization-dependent $T = T_{opt}$ and $n = n_{opt}$. However, we found that this approach does not lead to a significant improvement in our results. This must be related to the fact that the dependence of the probability to measure the state with the maximum $|E_j|$ on n is rather smooth

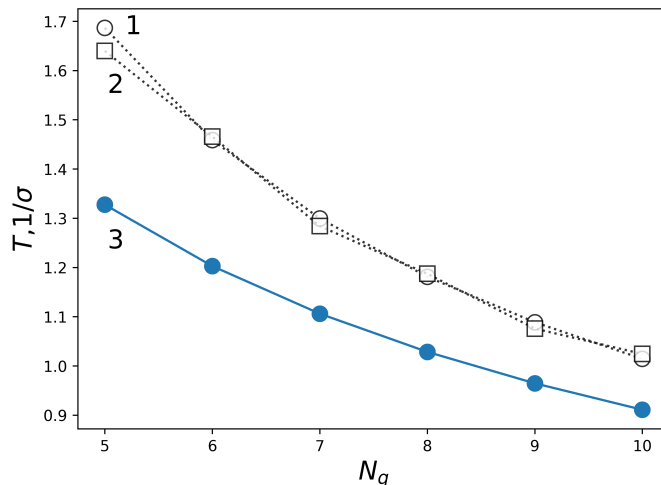


Fig. 8: The optimal evolution time versus qubit number N_q : calculated numerically and averaged over 100 realizations of disorder (curve 1), found numerically from the solution of Eq. (9) (curve 2), determined by the asymptotic expansion (12) (curve 3). Lines are guides for eyes connecting discrete points.

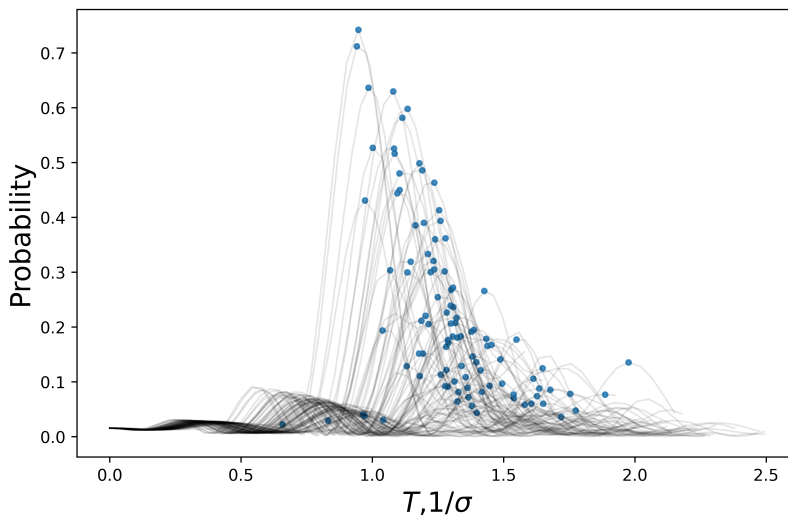


Fig. 9: The probability of the measuring the state with the maximum $|E_j|$ as a function of time T for $N_q = 6$ and 100 realizations of disorder.

in the vicinity of n^* , as expected for Grover's search.

IV. CONCLUSIONS

In this paper, we have introduced a theoretical framework based on Grover's search, which can be effectively employed for the quantum simulation of Ising models and similar classical spin systems. Specifically, we have illustrated the fundamental concepts of our approach using the Ising model characterized by all-to-all interactions and random energy constants.

Central to our methodology is the utilization of the evolution operator for the Ising model as a quantum oracle within Grover's search algorithm. This operator, when applied to the uniform superposition of all eigenstates of the Hamiltonian, induces phase shifts dependent on eigenenergies and evolution time. By carefully selecting an optimal

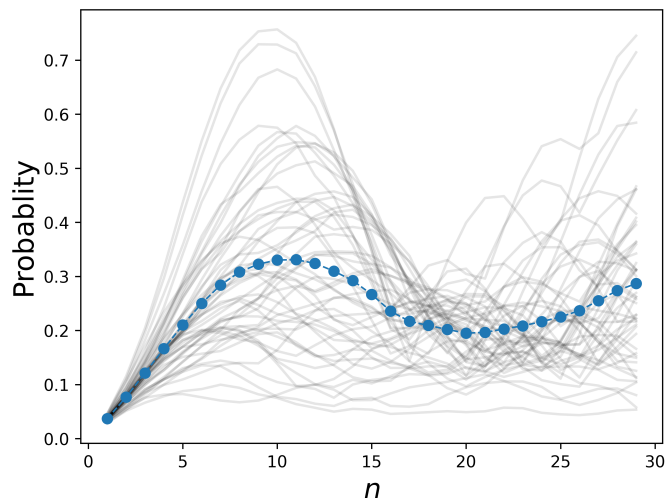


Fig. 10: The probability of measuring the state with the maximum $|E_j|$ at optimal time $T = T_{opt}$ for different Grover's iteration numbers n , $N_q = 7$, and 50 realizations of disorder. Blue dots show data averaged over the realizations of disorder. Blue dashed line is guide for eyes connecting discrete points.

evolution time, which effectively flips the sign in front of the state with the target energy, we can enhance the probability of finding this state through Grover's search.

We have applied these principles to the task of identifying the lowest or highest energy states (or other states with closed energies) for disordered Ising models, a problem that becomes exponentially complex as the number of spins increases. Through our demonstrations, we have elucidated the fundamental operational principles of our approach.

Acknowledgments

Useful discussions with M. A. Remnev are acknowledged. W. V. P. and A. V. L. acknowledge support from the RSF grant No. 23-72-30004 (theoretical formalism) and from the grant of the Ministry of Science and Higher Education of the Russian Federation No. 075-15-2024-632 dated June 14, 2024 (numerical experiments).

Data availability

The data used in the current study is available upon reasonable request from the corresponding authors. The code used can be found at <https://zenodo.org/records/12697641>.

-
- [1] L. Postler, S. Heussen, I. Pogorelov, M. Rispler, T. Feldker, M. Meth, C. D. Marciniak, R. Stricker, M. Ringbauer, R. Blatt, et al., *Nature* **605**, 675–680 (2022).
 - [2] Y. Kim, A. Eddins, S. Anand, K. X. Wei, E. Van Den Berg, S. Rosenblatt, H. Nayfeh, Y. Wu, M. Zaletel, K. Temme, et al., *Nature* **618**, 500 (2023).
 - [3] D. Bluvstein, S. J. Evered, A. A. Geim, S. H. Li, H. Zhou, T. Manovitz, S. Ebadi, M. Cain, M. Kalinowski, D. Hangleiter, et al., *Nature* (2023).
 - [4] R. Acharya, I. Aleiner, R. Allen, T. I. Andersen, M. Ansmann, F. Arute, K. Arya, A. Asfaw, J. Atalaya, R. Babbush, et al., *Nature* **614**, 676–681 (2023).

- [5] Y. Manin, Sovetskoye Radio, Moscow **128**, 28 (1980).
- [6] R. P. Feynman, International Journal of Theoretical Physics **21**, 467–488 (1982).
- [7] M. A. Nielsen and I. L. Chuang, *Quantum computation and quantum information* (Cambridge university press, 2010).
- [8] P. W. Shor, SIAM review **41**, 303 (1999).
- [9] L. K. Grover, in *Proceedings of the twenty-eighth annual ACM symposium on Theory of computing* (1996), pp. 212–219.
- [10] Y. Wang and P. S. Krstic, Phys. Rev. A **102**, 042609 (2020).
- [11] G. Anikeeva, O. Marković, V. Borish, J. A. Hines, S. V. Rajagopal, E. S. Cooper, A. Periwal, A. Safavi-Naeini, E. J. Davis, and M. Schleier-Smith, PRX Quantum **2**, 020319 (2021).
- [12] H. Tezuka, K. Nakaji, T. Satoh, and N. Yamamoto, Phys. Rev. A **105**, 032440 (2022).
- [13] T. Roy, L. Jiang, and D. I. Schuster, Phys. Rev. Res. **4**, L022013 (2022).
- [14] M. E. S. Morales, T. Tlyachev, and J. Biamonte, Phys. Rev. A **98**, 062333 (2018).
- [15] A. Lucas, Frontiers in Physics **2** (2014).
- [16] N. Mohseni, P. L. McMahon, and T. Byrnes, Nature Reviews Physics **4**, 363–379 (2022).
- [17] T. Kadowaki and H. Nishimori, Phys. Rev. E **58**, 5355 (1998).
- [18] G. E. Santoro, R. Martonák, E. Tosatti, and R. Car, Science **295**, 2427 (2002).
- [19] R. Barends, A. Shabani, L. Lamata, J. Kelly, A. Mezzacapo, U. L. Heras, R. Babbush, A. G. Fowler, B. Campbell, Y. Chen, et al., Nature **534**, 222–226 (2016).
- [20] M. Cerezo, A. Arrasmith, R. Babbush, S. C. Benjamin, S. Endo, K. Fujii, J. R. McClean, K. Mitarai, X. Yuan, L. Cincio, et al., Nature Reviews Physics **3**, 625–644 (2021).
- [21] J. Tilly, H. Chen, S. Cao, D. Picozzi, K. Setia, Y. Li, E. Grant, L. Wossnig, I. Rungger, G. H. Booth, et al., Physics Reports **986**, 1–128 (2022).
- [22] Y. Wang and P. S. Krstic, Phys. Rev. A **102**, 042609 (2020).
- [23] C. Bybee, D. Kleyko, D. E. Nikonov, A. Khosrowshahi, B. A. Olshausen, and F. T. Sommer, Nat. Commun. **14**, 6033 (2023).